



HAL
open science

Experimental and numerical analysis of seat belt bunching phenomena

David Dubois, Harald Zellmer, Eric Markiewicz

► **To cite this version:**

David Dubois, Harald Zellmer, Eric Markiewicz. Experimental and numerical analysis of seat belt bunching phenomena. *International Journal of Impact Engineering*, 2009, 36 (6), pp.763. 10.1016/j.ijimpeng.2008.11.006 . hal-00573076

HAL Id: hal-00573076

<https://hal.science/hal-00573076>

Submitted on 3 Mar 2011

HAL is a multi-disciplinary open access archive for the deposit and dissemination of scientific research documents, whether they are published or not. The documents may come from teaching and research institutions in France or abroad, or from public or private research centers.

L'archive ouverte pluridisciplinaire **HAL**, est destinée au dépôt et à la diffusion de documents scientifiques de niveau recherche, publiés ou non, émanant des établissements d'enseignement et de recherche français ou étrangers, des laboratoires publics ou privés.

Accepted Manuscript

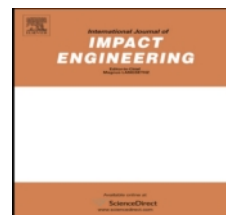
Title: Experimental and numerical analysis of seat belt bunching phenomena

Authors: David Dubois, Harald Zellmer, Eric Markiewicz

PII: S0734-743X(08)00309-6

DOI: [10.1016/j.ijimpeng.2008.11.006](https://doi.org/10.1016/j.ijimpeng.2008.11.006)

Reference: IE 1720



To appear in: *International Journal of Impact Engineering*

Received Date: 6 May 2008

Revised Date: 6 November 2008

Accepted Date: 10 November 2008

Please cite this article as: Dubois D, Zellmer H, Markiewicz E. Experimental and numerical analysis of seat belt bunching phenomena, *International Journal of Impact Engineering* (2008), doi: [10.1016/j.ijimpeng.2008.11.006](https://doi.org/10.1016/j.ijimpeng.2008.11.006)

This is a PDF file of an unedited manuscript that has been accepted for publication. As a service to our customers we are providing this early version of the manuscript. The manuscript will undergo copyediting, typesetting, and review of the resulting proof before it is published in its final form. Please note that during the production process errors may be discovered which could affect the content, and all legal disclaimers that apply to the journal pertain.

Experimental and numerical analysis of seat belt bunching phenomena

David Dubois^a, Harald Zellmer^b, Eric Markiewicz^c

^aAutoliv France, Avenue de l'Europe, 76220 Gournay en Bray, France

^b Autoliv Germany, Otto-Hahn-Strasse 4, P O Box 109, D-25333 Elmshorn, Germany

^c University of Valenciennes, Laboratory of Industrial and Human Automation Control, Mechanical Engineering and Computer Science LAMIH UMR CNRS 8530, Le Mont Houy, Jonas 2, 59313 Valenciennes, Cedex 9, France

Abstract

In current cars, loops are commonly used to redirect the webbing which reels out from the retractor to the passenger's shoulder. Some types of pillar loops, also called D-rings, lead to a non-systematic instability. The webbing, which should scroll without hindrance through the D-ring, laterally shifts, bunches and produces the overturning of the ring.

In this paper, this so-called seat belt bunching phenomenon is parsed during a first step with sled test campaigns data. The results of designs of experiments are analysed and discussed.

To expertise this instability issue, an innovative fixture is exploited during a second step to reproduce the phenomenon in a fully controlled manner for dynamic and quasi-static loadings. To assess these sub-system tests, a Digital Images Correlation system is employed to evaluate the strain distribution of seat belt webbing during the bunching phase. Based on these local measurements, a correlation of a Finite Element model of seat belt bunching is achieved using a new shell element for webbing fabric, before proposing an explanation of the phenomenon.

Keywords: Seat Belt; Bunching; Finite Element; Correlation

1. Introduction

Automotive manufacturers and suppliers commonly conduct crash tests in order to assess the performance of safety systems on new vehicles. Crash scenarios are reproduced using dynamic tests. For instance, the EuroNCAP protocol; a 64 km/h frontal impact in a 40% offset deformable barrier is used to simulate a car to car impact. An assessment protocol is then applied to achieve a rating for each body region. The head acceleration, the chest deflection, the femurs loading, compression / extension / flexion of the neck are measured on crash test dummies and a star rating is given. The safest cars obtain a 5 star performance.

During the vehicle deceleration, the dummies are subjected to the collision forces and in the case of a frontal impact, they move forward. To prevent severe contacts between the passenger and the car interior (dashboard, steering wheel), a three-point seat belt restrains the passenger's motion. In parallel, the driver and the passenger airbags reduce the acceleration peak applied to the occupant and distribute the restraint loads on the upper part of the body. To take benefit of their coupled actions, these restraint systems are developed in interaction. Nevertheless, although an airbag has a spectacular action during a collision, the belt, part of the passive restraint system, is the only protection against the ejection of the passenger away from his vehicle.

A safety belt webbing is a fabric material using polyester threads woven on Jacquard weaving looms. The webbing of a width of 48 mm of the belt restraint system has to resist to dynamic loads up to 14kN. Depending on the type of vehicle, about 3.5m of webbing are used in the seat belt. The interactions between the warp and weft threads of the fabric control the behaviour of the seat belt during the crash event.

Seat belt systems are usually combined with a load limiter retractor and also pretensioner integrated in the retractor, fixed at the buckle or at the lower part of the B

pillar (the pillar on which the rear doors are fixed). A D-ring is used on the upper part of this pillar in order to redirect the seat belt, which reels out from the retractor to the passenger shoulder. It is designed to adapt its angular position according to the passenger's motion. Numerous different kinds of D-rings (also called webbing guides) are used in current vehicles: most of them are made of a metal insert on which polymer part in nylon or in acetyl is moulded (see Fig. 1.a). In some cases, the ring frame and the guidance surface are made of one piece of metal (see Fig. 1.b). In the latest vehicles, the complete webbing guide assemblies are integrated into the trim panel, and only the diagonal belt portion appears (see Fig. 1.c).

For some belt geometries (the 3D position of the anchorage points of the seat belt on the vehicle), the use of certain D-rings has led to a non-systematic instability, which is very disadvantageous. The webbing, which should scroll without hindrance through the webbing guide, laterally shifts, bunches and produces the overturning of the ring as shown on

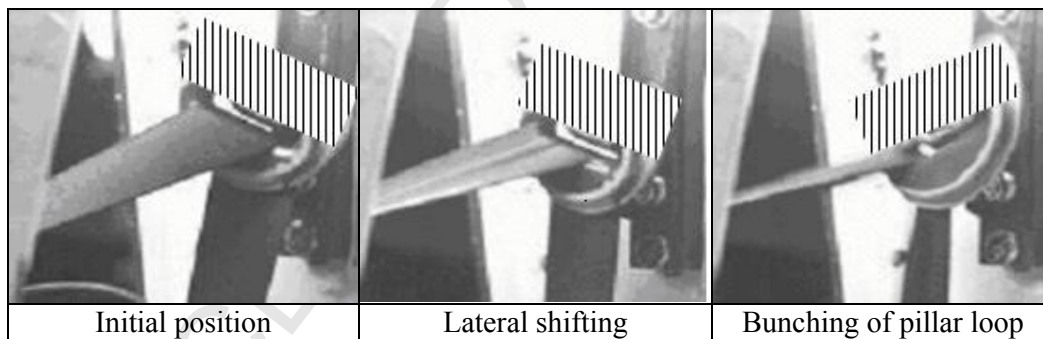


Fig. 2, where the D-ring has been masked for confidentiality reasons.

This phenomenon is an issue because it might prevent the restraint systems connected to the webbing from working in a normal manner (pre-tensioner, load limiter). In the face of such a problem, various studies [1], [2], [3], [4] have been carried out to control this phenomenon and needed to be pursued.

2. Analysis of the phenomenon based on sled tests

To develop restraint systems, numerical simulations are conducted and to confirm the airbag and the seat belt performances, dynamic sled tests are performed.

A sled is a mechanical welded assembly developed to simulate the car interior. The anchorage points of the seat belt are positioned in accordance with the car project specifications. The dashboard geometry is reproduced using foams and seat prototypes are used.

The bunching phenomenon was occasionally observed during these non-destructive sled tests. Previous studies [1] shown that during this type of tests, the plastic deformations of the crash frame are not reproduced and the corresponding absorbed energy is transferred to the webbing (no deformation of the B pillar on which the D-ring is fixed, no deformation of the car floor on which the seat is fixed, no dynamic pitch of the car body). The load applied to the seat belt webbing (measured locally by specific load cells) is thus often higher than the load measured during the corresponding complete vehicle crash tests. Sled tests are known to overload the webbing and to maximise the seat belt bunching likelihood.

To expertise belt behaviours, frontal sled tests campaigns were performed. Based on this experimental approach, designs of experiments have permitted to point out that one of the major factors which influence the phenomenon is the seat belt geometry [1]. Several risky seat belt geometries have been then defined but no generic assessment has been developed to explain the seat belt bunching phenomenon.

To pursue the research, a critical analysis of the design of experiments results was proposed. It appears that two consecutive and supposed identical tests may result in two different local behaviours of the ring (bunching for the first one and no bunching for the second one). For instance, sled tests performed with two seats on the same platform (and thus the same pulse, the same dummies, the same belt geometries) gave different

results: bunching on one side and no bunching on the other side (see Fig. 3). This status questioned the initial condition of the seat belt webbing and D-ring interactions. An analysis of the initial lateral position of the webbing on the D-ring has been then conducted (see

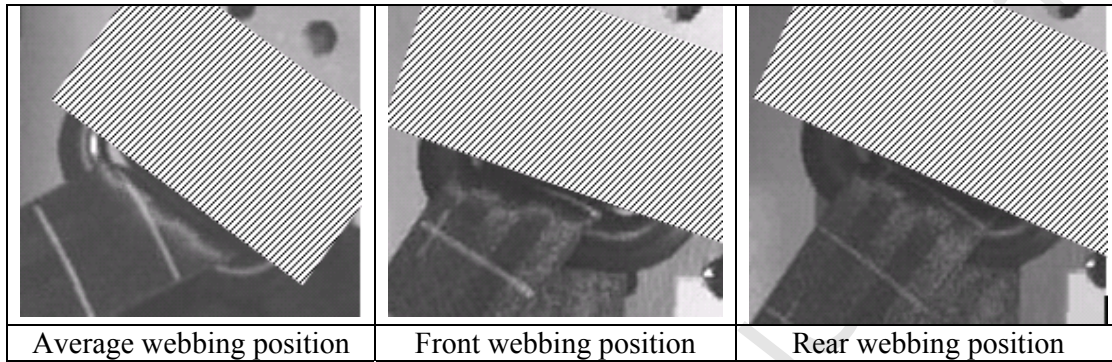


Fig. 4, where the D-ring has been masked for confidentiality reasons).

This critical analysis underlined an unexpected factor which influences the bunching likelihood, the initial position of the webbing according to the D-ring slot corners. A tiny variation of the webbing position can modify or delay the bunching phenomenon.

The initial positioning of the webbing on the D-ring was not known at first as being an influential factor on the crash test results because it is usually not a factor under control. Several points can explain this insufficiency:

- The initial position of the webbing on the D-ring is a consequence of the belt geometry. Moreover, the size of the dummy (Hybrid III 05, 50 or 95%^{ile}) and the seat position (slide position, height adjustment position) also vary the webbing/ D-ring boundary conditions.
- It is also controlled by component specification, the friction level between the D-ring and the webbing, the friction value between the webbing and the dummy, the spring strength inside the retractor and also the webbing slack resulting from the manual buckling of the seat belt on the dummy's body.

- The dynamic ring technology has also an influence on the webbing positioning on the D-ring. In a case of a direct crash test (sled decelerated using deformable bumpers), the initial webbing position is often modified by the tiny sways of the dummy during the acceleration phase. These perturbations can potentially be reduced by the use on an inversed crash sled (sled accelerated using hydraulic valves), but as the seat belt bunching phenomenon is an instability problem, small variations of the sled pulse can also interfere on the webbing behaviour.

The critical analysis of the results of designs of experiments shows that experimental studies based on sled tests are helpful to investigate the phenomenon but do not lead to a final solution to the instability of D-rings. They enable to list several important influential factors and to show tendencies. Detailed analysis proved that sled dynamic tests are not adapted to the study of the webbing/D-ring interactions, because this test method provokes local dispersions which have an effect on the final result of the experiments.

Numerous sled tests would be necessary to evaluate the trends according to the initial position of the webbing on the D-ring, but the high cost of these sled tests does not enable to pursue in that way.

3. Analysis of the phenomenon based on global sub-system tests

To complete the analysis of the seat belt bunching phenomenon, a global sub-system test, called Webbing Guide Drop Test (WGDT) has been used [5]. The principle of this bench is: a half cylinder drop weight, fixed to the sled of a drop test, impacts a horizontal webbing portion between a set of rods (see Fig. 5). The horizontal webbing portion is then pulled and the shoulder belt reels out. The D-ring is screwed on a vertical column. Its column is oriented at 45° to facilitate the shoulder belt orientation. The total energy applied to the system is controlled by the mass and the speed of the impactor.

Experimental campaigns showed that the WGDT is a consistent method to test D-ring in dynamic loading conditions. With this device, the D-ring's instability can be easily reproduced (see

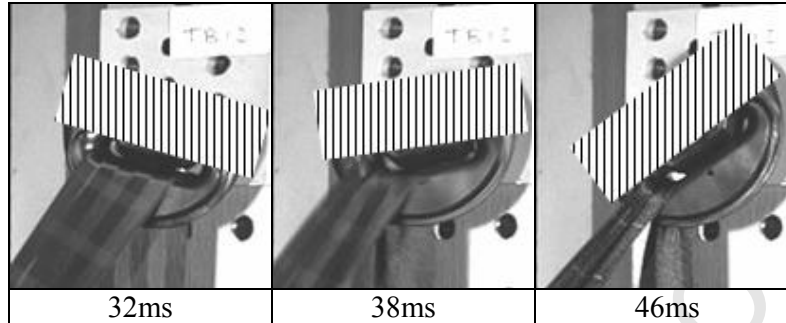


Fig. 6) with loading levels and scrolling speeds equivalent to those observed during R16 sled tests [6]. The advantage of this test method compared to sled test is that results are completely repeatable and the cost per experiment is low compared to dynamic sled tests.

The use of the WGDT to investigate the seat belt bunching phenomenon enables to complete the global understanding of the webbing behaviour. It confirms that the initial position of the webbing influences the global stability of the ring. Nevertheless to assess and to solve the ring's instability; a local analysis of the webbing has been investigated.

4. Analysis of the phenomenon based on local sub-system tests

Based on sled test results and the WGDT results, the need of a local sub system test has emerged [7].

4.1. Sub-System Test

To reduce the variance of designs of experiment based on sled test and to focus the study on the behaviour of D-rings, a sub-system test method has been used. Thus, an innovative experimental bench was developed by Autoliv North Germany [8], [9].

4.2. Experimental set-up

This innovative experimental bench called WGRAT (Webbing Guide Rotative Arm Test), consists in two main parts (see Fig. 7) fixed on a quasi-static tensile test machine:

- Part 1: a support structure with a rotating arm on which the D-ring is fixed.
- Part 2: a fixture on which the retractor and a load cell are mounted.

This mechanism has a multi-angle rotative arm, which allows to reproduce all the belt orientations seen in an automotive vehicle. It is usually fixed to the lower jaw of a tensile test machine. For each test, a retractor is mounted on the device, the D-ring is fixed on its axle and the webbing is set through the ring. Then, the free end of the webbing is fixed to the upper jaw of the tensile test machine. The experimental fixture (see Fig. 8) enables to load the D-ring in similar loading conditions to a sled test.

The use of two devices of angle variation allows re-creating the seat belt curvature through the D-ring. Compared to a real car set up, the loading conditions are varied as following:

- The position of the retractor and the position of the loading webbing end are reversed.
- The loading direction is constant (during a sled test, the dummy is moving forward and the loading direction is varying).
- The speed of loading is limited by the pulling device specification (it can reach up to several meters per second during a sled test).
- No deceleration pulse is applied to the D-ring and to the webbing.

5. Experimental analysis based on WGRAT

The local assessment on the seat belt bunching phenomena based on experimental tests has been pursued in two steps:

- For dynamic loadings, using an hydraulic jack and a high speed video camera.
- For quasi-static loadings, using a tensile test machine and a Digital Images Correlation for strain distribution measurement.

5.1. Dynamic WGRAT Test Set Up

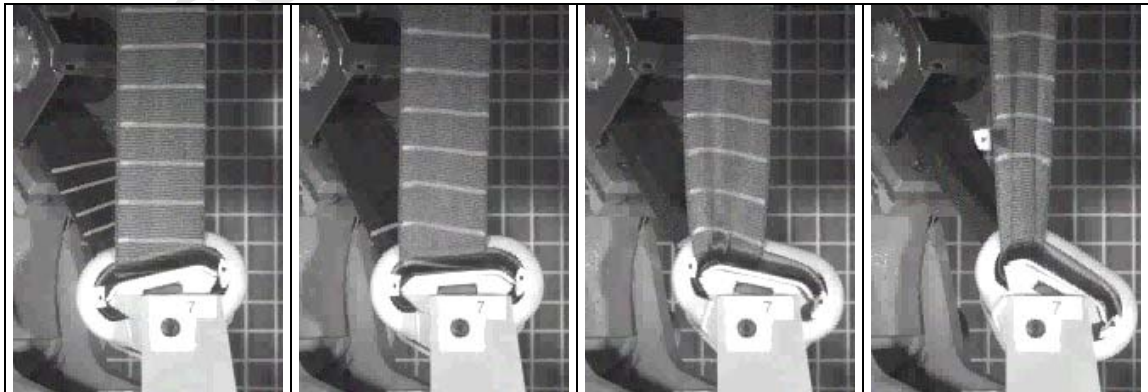
The WGRAT device was adapted to dynamic loadings to obtain the same outlet speed of the webbing through the webbing guide than the speed measured during dynamic sled tests (see Fig. 9).

Thus, the fixture was mounted on a high-speed hydraulic jack at ONERA Lab. Center of Lille (The French Aerospace Lab.). The frame is made of two vertical columns fixed on ground ($2.5 \times 2.5 \text{ m}^2$). This ground is fixed to a 40 tons seismic mass suspended and damped. The columns are connected by a horizontal crosspiece to two degrees of freedom, on the middle of which the hydraulic jack is mounted.

Its loading capacity is 50kN in dynamic. Its maximal speed is close to 10m/s. The cylinder travel exceeds 250mm. Its guidance is obtained by hydrostatic bearings and allows radial loadings.

5.2. Dynamic WGRAT Test Result

For a 200mm jaw displacement at 3.5m/s and a $45^\circ/45^\circ$ angle between the vertical belt and the diagonal belt, the webbing initially in a central position, slides laterally and bunches in the left corner of the ring at 22 ms (see



16ms	18ms	20ms	22ms
------	------	------	------

Fig. 10).

These dynamic tests enable to visualize the deformation of the vertical belt portion. Initially flat, the webbing deforms and several weaves appear on the surface close to the ring. In parallel, the analyses of horizontal lines drawn on the belt show discontinuous local perturbations which grow until bunching.

5.3. Quasi-static WGRAT test set up

During a second step, the WGRAT device has been used for quasi-static loadings to evaluate the strain distribution through the webbing (see Fig. 11). To complete the assessment of the seat belt bunching phenomena, an analysis of the strain distribution through the webbing during the instability issue has been investigated.

In order to study the strain field distribution over the seat belt webbing during the bunching phenomena, tensile tests, performed on an INSTRON™ tensile test machine, were undertaken and post-analysed by "GOM/ARAMIS™" Digital Images Correlation system [10].

To enable the strain measurement, the specimens needed to be prepared. For this purpose, a very thin layer of white flexible silicon was spread on the surface of the vertical portion of webbing. A black colour spray was next applied to obtain an irregular contrast pattern results.

During these quasi-static tests, the following set up was used:

- Retractor without load limiter (to reduce the reel out distance of the webbing through D-ring and to focus the analysis area).
- 45°/45° belt geometry.
- The webbing was positioned in the middle of the D-ring.
- The loading speed was fixed at 100 mm/min.
- The camera frame was fixed to one frame per second.

- A 1240*1240 pixels resolution digital video camera was used.

The sample was installed in the tensile testing machine and the ARAMIS system was calibrated and positioned in front of the sample (see Fig. 12). During the tensile tests, a camera recorded the 2D displacements of the splash pattern. During the same time, the displacement of the jaw, the tensile load and the retractor load were recorded.

A Digital Images Correlation of the movie pictures was performed to measure the longitudinal and transversal strain distributions. This method has enabled to quantitatively capture the development of an unbalanced strain field of the webbing before and during the bunching phenomenon.

5.4. Quasi-static WGRAT Test Results

Three repeatable tensile tests were performed. During these tests, left bunching phenomena occurred. The two main directions of the strain tensor were calculated and they showed different behaviours. The measurement field, size about 10 x 4 cm² was located in the center of the specimen where the largest deformation was expected. Finally, the deformation behaviour in the whole measuring area was observed in real-time until bunching.

By eliminating the jaw movement of the specimen, the local deformation of the specimen surface can be made visible. By a mathematical derivation of these images, the strains were determined and displayed as a whole field distribution (isolines of equal strains). The distribution epsilon X and epsilon Y was calculated and graphically shown by plotting strain curves variation exported in a specific ASCII-format. Thus, the behaviour of the sample during the test shall be evaluated and displayed graphically.

5.4.1. Transversal strain

The analysis of the deformation of the seat belt webbing (in the weft direction) shows a homogenous and a close to zero strain distribution of the webbing before the bunching phenomena. As soon as the webbing begins to bunch, the out of plane deformation of the samples disturbs the measurement.

5.4.2. Longitudinal strain

The analysis of the longitudinal strain of webbing shows that its behaviour varies in several stages:

From 0 to 34mm, a homogenous distribution of the longitudinal strain can be seen on the webbing sample (see Fig. 13).

- At 34mm, a dissymmetry of the longitudinal strain appears and this dissymmetry increases from 34 to 67mm. At that stage, the difference between the strain values calculated on the right edge and the ones calculated on the left edge of the webbing sample reaches 30%. (see Fig. 14).

This phenomenon was computed along several sections of the webbing (see sections 1 to 5, Fig. 14). An increasing difference reaching more than 2% of longitudinal strain value (a variation of 30% between each edge, see Fig. 15) was measured between the two edges of the webbing before the overturning of the D-ring.

- At 68mm, the bunching phenomenon begins, and 15mm later the bunching phenomenon is completely achieved (see Fig. 16).
- After bunching, at 83mm, the out of plane deformation of the sample disturbs the measurement in the center of the specimen but the edges deformation can be assessed. For each edge, the longitudinal strain reaches the same average value: 9% (see Fig. 17).

Judging from the results obtained by the Digital Image Correlation method, the phenomenology of the seat belt bunching phenomenon can be discussed:

At the beginning of the test, the belt is uniformly loaded, thus the system is in equilibrium. A disequilibrium appears, the longitudinal strain distribution becomes inhomogeneous along the width of the webbing. That unbalanced strain distribution grows up to reach a 30% variation between each edge of the webbing and leads to the instability of the system by the overturning of the D-ring. The system has reached a new stable state with a symmetric strain distribution.

At that stage, the dissymmetry of the strain distribution and the D-ring rotation appear to be synchronized. To complete the results obtained with the Digital Image Correlation method and to pursue the assessment of the bunching phenomena, a FE numerical model of D-ring / seat belt interactions has been developed. The use of this numerical tool aims at organizing into hierarchy the factors influencing on the stability of D-rings.

6. Numerical analysis based on WGRAT tests

To complete the experimental analysis of the seat belt bunching phenomena based on the WGRAT dynamic and quasi-static test results, a numerical analysis is proposed. A specific FE model of seat belt webbing is developed. Based on the numerical innovation, the experimental tests described in the previous chapter are modelled.

6.1. FE model – new shell finite element model for webbing

To improve the finite element model of seat belt webbing fabric, an innovative shell finite element is developed using Pam-CrashTM packages [11]. This shell element takes into account the low but effective bending stiffness of the seat belt webbing by the use of a plate bending element with a decoupled and orthotropic bending stiffness.

According to the results of tests on seat belt webbing, a method to simulate its

behaviour was studied. To evaluate its stability, it is applied to realistic belt geometries and loadings.

The global behaviour of seat belt webbings corresponds to the behaviour of a fabric. Fabrics are usually modelled with membrane elements, which do not take the bending stiffness into account. This method has proved to be satisfactory for the simulation of thin fabrics, such as fabrics used for airbags, but cannot be extrapolated to the case of seat belt webbing because the bending stiffness cannot be neglected during the bunching phenomenon.

Thus a new simulation method was used to model the behaviour of seat belt webbings. It consists in the superposition of two layers of shell finite elements (see Fig. 18.). The two layers are defined with the same nodes and the density of each layer corresponds to half the density of seat belt webbings.

The first layer is a membrane element usually used for fabric element; it defines the membrane behaviour. The first part of this model corresponds to the membrane stiffness. Its main use in the field of dynamics is the simulation of airbag fabric. This material corresponds to a linear elastic membrane material which consists in two families of fibres, running at given angles in two directions, embedded in an isotropic matrix. The following general relationship between membrane stresses and strains describes the general isotropic case.

fabric = isotropic matrix + layer 1 at 0° + layer 2 at 90°

$$\begin{bmatrix} \sigma_{11} \\ \sigma_{22} \\ \tau_{12} \end{bmatrix} = \left(\frac{Em}{1-\nu^2} \begin{bmatrix} 1 & \nu & 0 \\ \nu & 1 & 0 \\ 0 & 0 & (1-\nu)/2 \end{bmatrix} + \begin{bmatrix} E_1 & 0 & 0 \\ 0 & 0 & 0 \\ 0 & 0 & G_1 \end{bmatrix} + \begin{bmatrix} 0 & 0 & 0 \\ 0 & E_2 & 0 \\ 0 & 0 & G_2 \end{bmatrix} \right) \begin{bmatrix} \epsilon_{11} \\ \epsilon_{22} \\ \gamma_{12} \end{bmatrix} \quad (1)$$

Where E_m is the Young's Modulus of the isotropic matrix, E_1 and E_2 are Young's tension/compression moduli of the threads, G_1 and G_2 are shear moduli and ν is the Poisson's coefficient.

This element is formulated in a total Lagrangian approach, in which the Green-Lagrange strains ($\epsilon_{GL} = 1/2 (L^2 - L_0^2) / L_0^2$) and the second Piola-Kirchhoff stresses are used ($\sigma_{PK} = (L/L_0) E \epsilon_{GL}$). This element is completely integrated by four Gaussian points.

The second part of the model corresponds to a bending plate stiffness based on a Mindlin shell element [12]. That plate bending element [11] is usually used in the field of non-linear dynamic loadings to simulate the behaviour of composite ply made of two components, the fibres and a matrix.

Then, the behaviour of uni-directional continuous fibres reinforced composites is modelled with this shell using the superposition of plies composed of two phases: a uni-directional fibres phase and an orthotropic matrix phase (see Fig. 19). The original aspect of this numerical model is the distinction of these two phases.

Each phase of each ply is defined independently in tension and in compression. For each ply, the stiffness is calculated by superposing the effects of the orthotropic elastic matrix (matrix minus fibres) and of the one-dimensional elastic fibres (see Fig. 20).

Within the context of the seat belt webbing, only the matrix phase has been used (no fibres phase has been used). To transform it into a bending plate stiffness, this shell element was degenerated by removing from the code the calculated membranes forces transmitted to the nodes (see Fig. 21).

Once superposed, the resulting layered element is thus a multi-layered quadrangle element (Q4) with a decoupled and orthotropic bending stiffness. The orthotropic

material phase is defined with the following strain-stress relation (expressed in the directions of orthotropy).

$$\begin{bmatrix} \sigma_{11} \\ \sigma_{22} \\ \tau_{12} \\ \tau_{13} \\ \tau_{23} \end{bmatrix} = \begin{bmatrix} C_{11} & \nu_{21}C_{11} & 0 & 0 & 0 \\ \nu_{12}C_{22} & C_{22} & 0 & 0 & 0 \\ 0 & 0 & G_{12} & 0 & 0 \\ 0 & 0 & 0 & G_{13} & 0 \\ 0 & 0 & 0 & 0 & G_{23} \end{bmatrix} \begin{bmatrix} \varepsilon_{11} \\ \varepsilon_{22} \\ \gamma_{12} \\ \gamma_{13} \\ \gamma_{23} \end{bmatrix} \quad (2)$$

With $C_{11} = \frac{E_{11}}{1 - \nu_{12} \cdot \nu_{21}}$ $C_{22} = \frac{E_{22}}{1 - \nu_{12} \cdot \nu_{21}}$ and $\frac{\nu_{12}}{E_{11}} = \frac{\nu_{21}}{E_{22}}$

Where: E_{11} the Young's modulus in direction 1

E_{22} the Young's modulus in direction 2

G_{12} the in-plane shear modulus

G_{13}, G_{23} the transversal shear moduli

$\nu_{n,m}$ the Poisson's ratio in n,m directions

This plate-bending element (12 d.o.f.) defines two different bending stiffnesses, in the warp and in the weft directions, independently of the membrane stiffness.

The parameters of the stiffness matrix were identified with rheological tests performed on seat belt webbing fabric [13]. Several experimental tests were undertaken:

- Picture frame tests to measure the real in plane shear modulus
- Cantilever tests to evaluate the bending stiffness
- Tensile tests for Young's modulus and the Poisson's ratio

This new shell finite element was used to simulate the behaviour of seat belt webbing and to investigate the webbing kinematics observed experimentally.

6.2. Numerical model of Dynamic WGRAT test

A numerical model has been achieved to reproduce the seat belt bunching cases which had been experimentally obtained. Special care has been devoted to model the tribology of the phenomenon in a most correct way.

6.2.1. Model development

A model is achieved to reproduce numerically the seat belt bunching cases experimentally obtained. The belt orientation ($45^\circ/45^\circ$) used during the experimental test campaign was reproduced using pre-simulations. At one end of the webbing, the Pam-SafeTM model of retractor is used to simulate the spool-out effect of the webbing on its spindle and to take into account the load limiting device existing in the retractors used during the tests set. At the other end, the loading method used for this simulation is an imposed displacement applied to the nodes of the free edge of the webbing (see Fig. 22). The "displacement / time" law used corresponds to the one measured at the pressure cylinder during the dynamic WGRAT tests.

The original aspect of this test is that the retractor is near the D-ring. In order to obtain a realistic simulation, a fixed cylinder (called "rigid wall") is used to reproduce the scrolling conditions of the webbing out from the retractor.

6.2.2. Friction Model

As the friction between belt webbing and D-ring rod may play a significant role in webbing instability, an in-depth analysis of the friction has been performed.

Safety belts are now generally woven out of Polyester. To improve the properties in slip and the abrasion resistance, a new generation of webbing is produced with polyester threads without torsion. The use of threads without torsion reduces the friction resistance because the filaments are strongly directed in the longitudinal direction.

The safety belts are woven according to a cross weave (2x2) in which, each wire passes above two consecutive weft threads then above two following weft threads. From a macroscopic point of view as the Jacquard weaving mode being directed, the surface quality in the weft and warp directions differs (see Fig. 23). The longitudinal and transversal tribologies are then different.

D-rings are often made of a metal insert on which polymer part (HostaformorTM, DelrinTM, etc.) is moulded. As polymeric materials badly hold the heat, the scrolling of the webbing on the D-ring dissolves the sliding surface (the melting point is lower than 200°C) and modifies the tribology.

The analysis of the webbing after loading shows that the polymer melts after some centimeter of scrolling (see Fig. 24). A molten polymer film is formed between the webbing and the ring. That phenomenon reduces the friction coefficients and homogenizes its value in the warp and weft directions.

Several D-ring types have been experimentally tested (see Fig. 25). D-rings with sheeted lines on the sliding surface or with a PTFE coating (teflonTM) on metal ring have shown the same seat belt bunching behaviour.

The smooth contact algorithm (type 46) from Pam-CrashTM data base [14] has been used to manage the sliding of the webbing on two smooth surfaces extrapolated from the surface nodes to avoid perturbations through the belt forces. This algorithm ensures the contact between the webbing and the D ring, and the self-contact of the webbing when bunching occurs (see Fig. 26).

A contact thickness defines a volume around the meshes of the webbing and the D ring. As soon as a node is entering this zone, a contact force is generated. A penalty method is used, for which the penetrations are allowed but penalized. The penalty force is linearly proportional to the depth of penetration. The interpenetration check frequency has been fixed to 1000 cycles to stabilize the contact.

$$F_{\text{contact}} = k \cdot \text{penetration}$$

$$\text{where } k = 0.1 \times k_{\text{stable}}$$

and k_{stable} is the stable stiffness to integrate with the given time step.

For a simplified 1 degree of freedom (see Fig. 27)

$$k_{\text{stable}} = M1.M2/(M1+M2). (1/Dt^2)$$

To model the friction, several friction models have been alternatively tested.

Isotropic Standard Coulomb Friction, orthotropic, pressure and/or velocity dependent friction models have been numerically evaluated.

Due to the molten polymer film between the webbing and the D-ring, a homogenized isotropic friction has been first chosen.

Pressure and velocity dependent friction models haven't proved significant improvement in the correlation process. As the modeled kinematics is an energetic and quick process, the melted state of the polymer is rapidly established and the dynamic friction value remains low during the whole loading.

Starting from the academic value of PTFE friction coefficient [15] equals to a 0.05, a parametric study has been performed to analyze the effect of the friction value variation (between 0.0 and 0.1) on the global kinematics of bunching. In that range, the overturning of the rings was equivalent. Preliminary results of a design of experiment, in which geometrical and physical parameters were varied, have also confirmed its low influence.

6.2.3. Model results

Based on the previous analysis, the friction between the webbing and the D-ring has been modelled using a coulomb friction fixed at a usual value of 0.05.

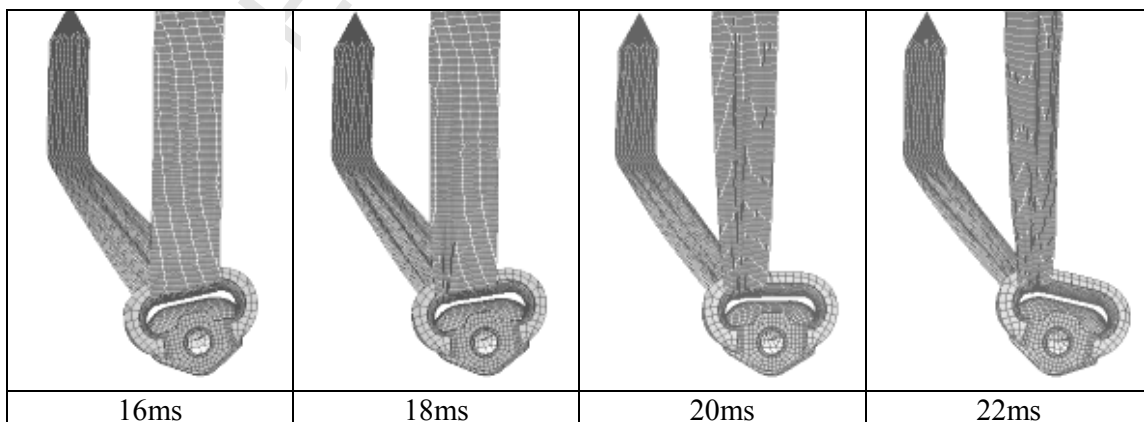


Fig. 29 shows several steps of a corresponding numerical seat belt bunching phenomenon obtained for a 45°/45° belt orientation.

The validation of the model is obtained by the comparison of the load levels through the webbing versus the webbing's end displacement measured experimentally and calculated by simulation (see Fig. 28).

The same global behaviour experimentally observed has been numerically reproduced (see

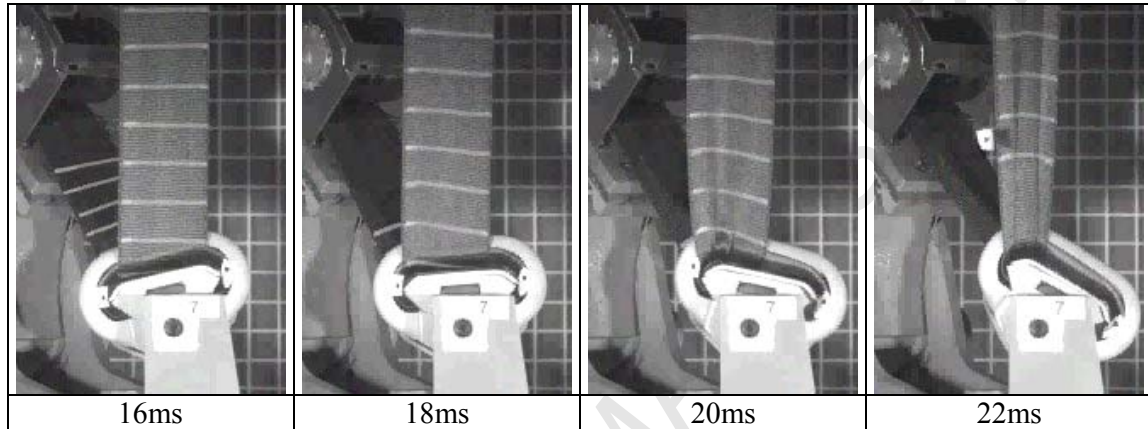


Fig. 10). Weaves on the webbing can be seen before bunching. A fine post-processing has been carried out to compare the strain distribution through the FE webbing to the one visualized experimentally using the previous "GOM/ARAMISTM" Digital Images Correlation method.

The numerical simulation is conducted as an adiabatic process; then, there is no heat transfer between the webbing and the D-ring. As the thermodynamics effects are not modelled, there is no modification of the sliding friction coefficient during Finite Elements runs. The effect of the inertial forces is also neglected between quasi-static and dynamic tests. Despite these strong hypotheses, the local phenomena are studied.

The comparison of the strain distribution fields obtained for two different velocities of loadings (experimentally in quasi-static loading see Fig. 14, numerically in dynamic loading see Fig. 30) shows the same strain dissymmetry.

Thus, the results of FE model show that the strain distribution is equivalent to the experimental measurement. At 17ms, the range of strain deformation between the two edges of the webbing extends from 6 to 8% (a variation of about 30%) and the iso-strain areas are localized in the same zones. At 22ms, after belt bunching, the overturning of the D-ring interrupts the disequilibrium. A new homogenous distribution of longitudinal strains (about 9%) can be observed on the vertical belt portion.

A design of experiment will be performed based on this correlated numerical model. That numerical study will take into account:

- The friction coefficient between the webbing and the D-ring.
- The bending stiffness of the webbing.
- The behaviour of the revoluted joint of the loop.

The aim of this analysis will be an improvement of the stability of the D-ring.

Numerical simulation data enable to complete experimental tests results and to assess the chronology of the phenomena. Up to the round off load value of 4kN, the webbing/D-ring couple is stable. The webbing reels out normally and the angular D-ring position is constant. Beyond that load level, the diagonal portion of the webbing shifts laterally on its guide. That shifting causes a dissymmetry of the D-ring loading which generates an angular rotation. That rotation imbalances the strain distribution of the webbing. In order to reduce this perturbation, the webbing's shifting grows. The two phenomena become coupled and quicken until the complete overturning of the ring.

7. Conclusion

The objective of this study was to assess the Seat Belt Bunching Phenomenon and to develop a numerical model of the instability issue. In this paper, the webbing / D-ring behaviour is first investigated using several experiments. An analysis of dynamic

sled tests results is proposed. Innovative global and local sub-system tests are developed and are used to investigate the overturning of the ring.

An efficient Finite Element model for seat belt webbing is developed using an original two layers shell quadrangle. The first layer is a membrane element usually used for fabric element. The second layer corresponds to a degenerated bending plate stiffness. Once superposed, the resulting layered element is a multi-layered quadrangle element with a decoupled and orthotropic bending stiffness.

FE models of the sub-system tests are developed using the layered shell element. The correlation of these finite element models is proved to be good. A fine post processing of the local subsystem test results is used to assess the behaviour of seat belt webbing. The internal strain distribution of the webbing measured by Digital Image Correlation is very well reproduced by the FE model and a numerical bunching phenomenon has been detected for an equivalent loading.

Based on experimental and numerical data, an assessment of the phenomenon is proposed. To complete this research study, further investigations are planned. This validated model will be used for a numerical Design of Experiment in order to analyze the stability of the D-ring and to fully control the bunching phenomenon.

Acknowledgements

The authors would like to thank Jacky Fabis from ONERA Lab Centre of Lille for his valuable contribution during the WGRAT tests.

References

- [1] D. Dubois, Master of Research, Simulation Project, Autoliv UK, Valenciennes University, LAMIH UMR 8530, Laboratory of Industrial and Human Automation Control, Mechanical Engineering and Computer Science, 2000.
- [2] Pedrazzi, Elsäßer and Schaub, TRW Occupant Restraint Systems Gmbh & Co, KG, Alfdorf, Simulation of belt movement in the D-ring during a crash CAD-FEM, User's meeting Internationale FEM-Technologietage Graf-Zeppelin-Haus, Friedrichshafen, 2000.
- [3] Pedrazzi, Elsäßer and Schaub, TRW Occupant Restraint Systems Gmbh & Co, KG, Alfdorf, Aspects of Seat belt Material Simulation, Third European LS-DYNA Conference, Dynalis, Paris, 2001.
- [4] D. Dubois, F.E. Analysis of Seat Belt Behaviour Under Dynamic loading, ICD2003, Int. Crashworthiness and Design Congress, Lille, 2003.
- [5] D. Dubois, H. Cord, E. Markiewicz, Innovative test method for seat belt D-ring, International Journal of Vehicle Safety, Vol.2, Nos. 1/2, 2007, p.87-102.
- [6] UNECE agreement, Addendum 15 Regulation 16, Safety-belts and restraint systems for occupants of power-driven vehicles, 1995.
- [7] D. Dubois, Prevention and Prediction of the Seat Belt Bunching Phenomena, PhD Thesis, University of Valenciennes, France, 2004.
- [8] P. Markvardsén, Experimentelle Untersuchung des Verhaltens von Sicherheitsgurtumlenkern in Frontalcrashverlauf, Autoliv North Germany, Internal report, 1999.
- [9] P. Markvardsén, Untersuchung einer neuentwickelten Prüfvorrichtung zur Simulation von Sicherheitsgurtumlenkern unter Lastbedingungen, Autoliv North Germany, Internal report, 2001.
- [10] Aramis, version 4.6.5, Fundamentals Principles, chapter 2, 2001, p.7-20.

- [11] Pam-Crash/Safe™, Solver Notes Manual, V2007, Shell/Membrane Materials, 2007, p. 253-348.
- [12] Mindlin R.D, Influence of Rotary Inertia and Shear on Flexural Motions of Isotropic, J.Applied Mechanics18, 1951, p.31-38.
- [13] D. Dubois, P. Gross, A. Trameçon, E. Markiewicz, F.E. analysis of seat belt bunching phenomena, International Journal of Crashworthiness, ISSN: 1358-8265 Vol. 11, Nos 6, 2006, p. 519-528.
- [14] Pam-Crash/Safe™, Solver Notes Manual, V2007, Shell/Membrane Materials, 2007, p. 562.
- [15] Gieck, Formulaire technique, ISBN : 3-920-379-24-1,1997, p. Z7.

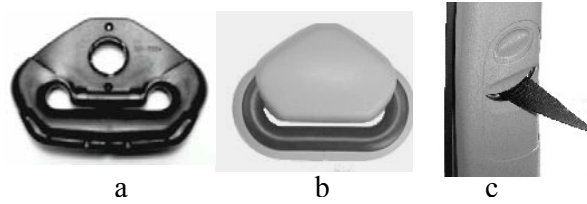


Fig. 1. Webbing Guides (courtesy Autoliv)

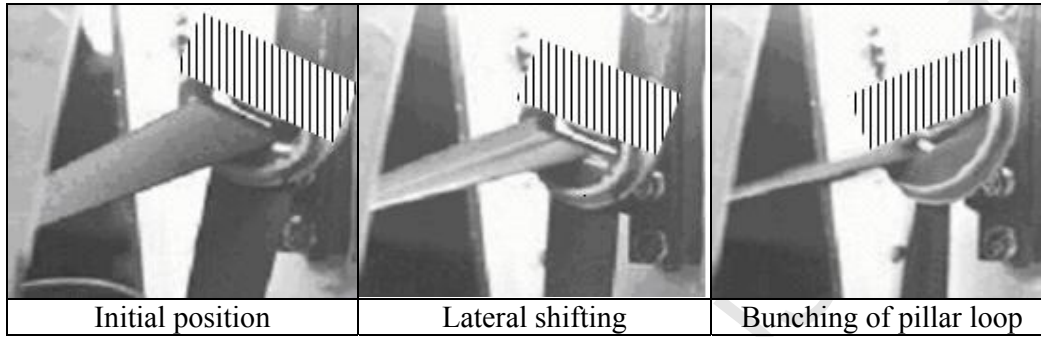


Fig. 2. Seat Belt Bunching Phenomenon



Fig. 3. Sled Test with two Hybrid III 95%ile dummies

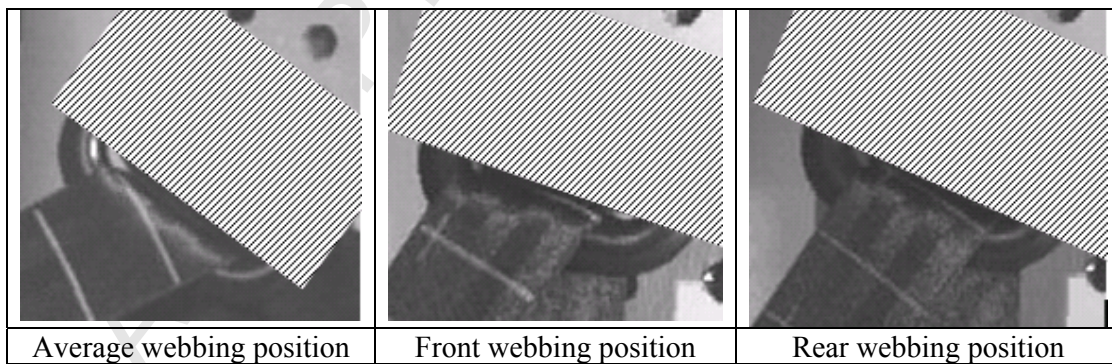


Fig. 4 Initial lateral positions of the webbing on the D-ring

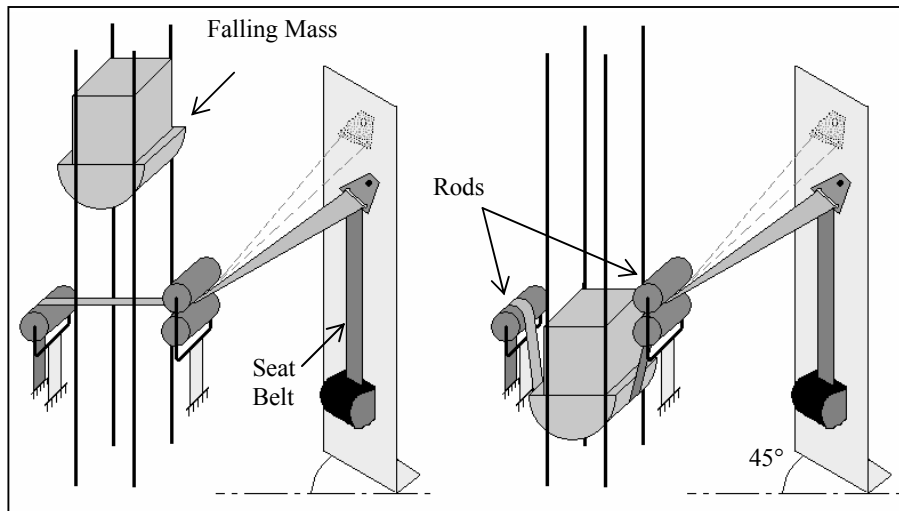


Fig. 5. WGDT principle

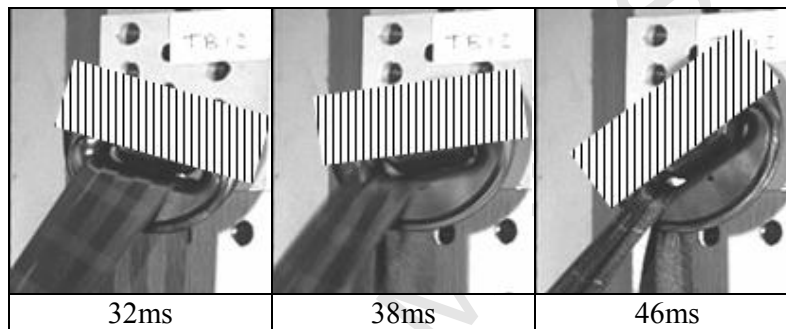


Fig. 6. Bunching phenomenon generated with the WGDT

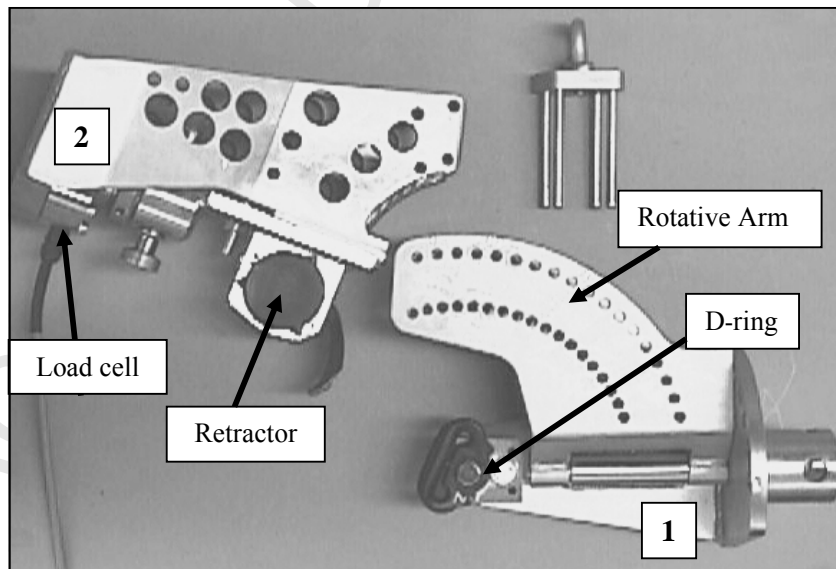


Fig. 7. Components of the WGRAT

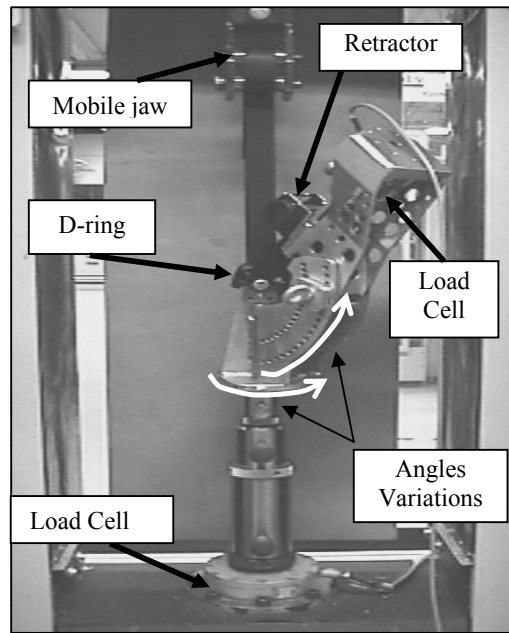


Fig. 8. WGRAT mounted on a quasi-static tensile test machine



Fig. 9. Experimental fixture mounted on a high-speed hydraulic jack at ONERA-Lille

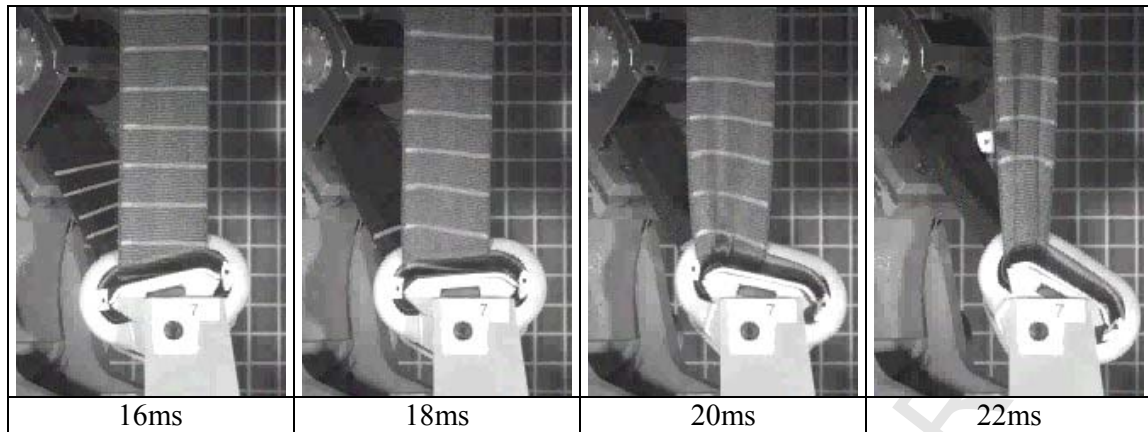


Fig. 10. Experimental case of bunching with the WGRAT

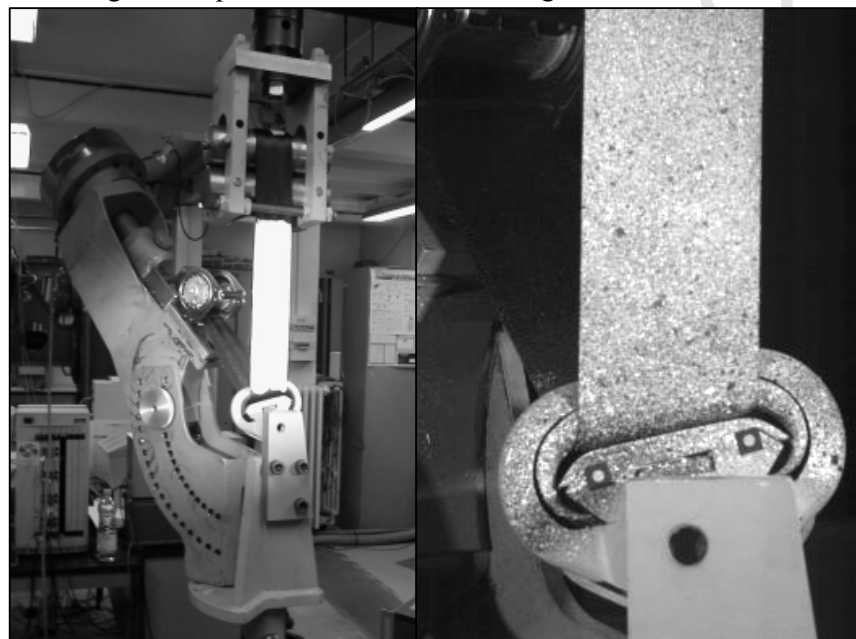


Fig. 11. Sample with splash pattern during a tensile test



Fig. 12. Camera of the ARAMIS measuring system and lights

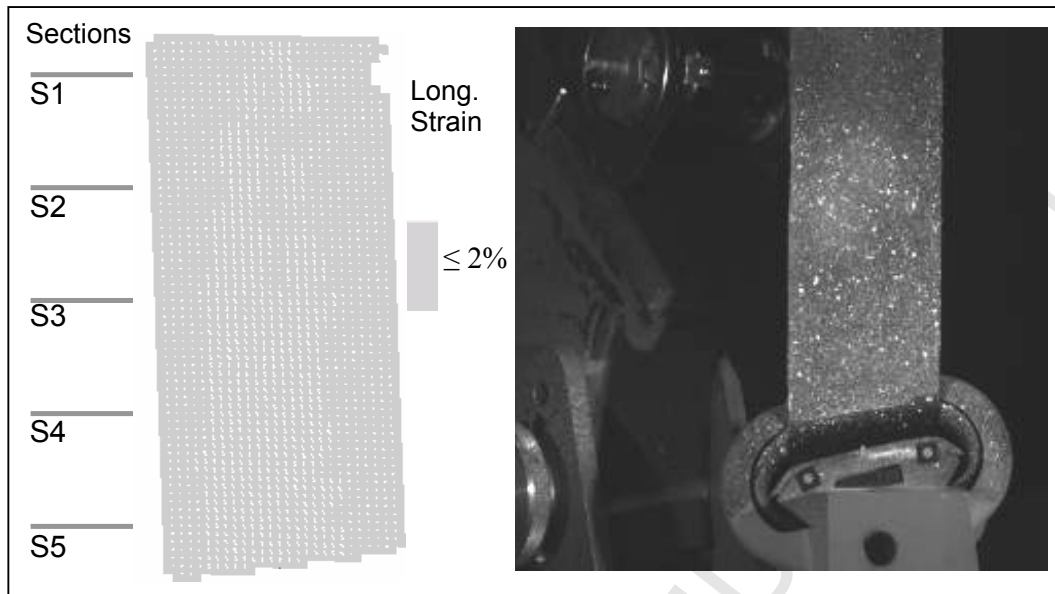


Fig. 13. Variation of the longitudinal strain distribution at 16mm

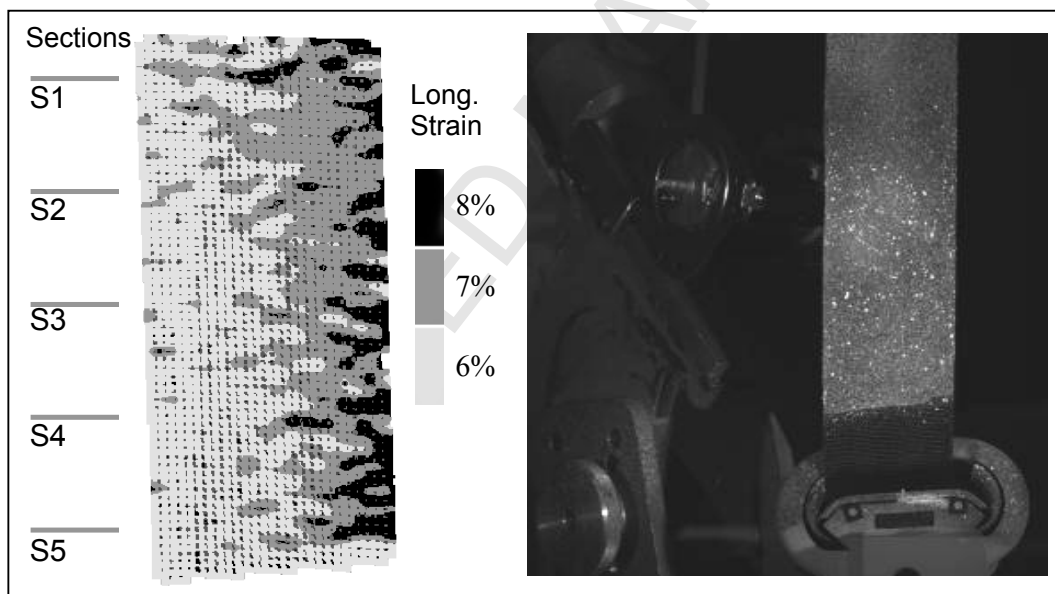


Fig. 14. Variation of the longitudinal strain distribution at 67mm

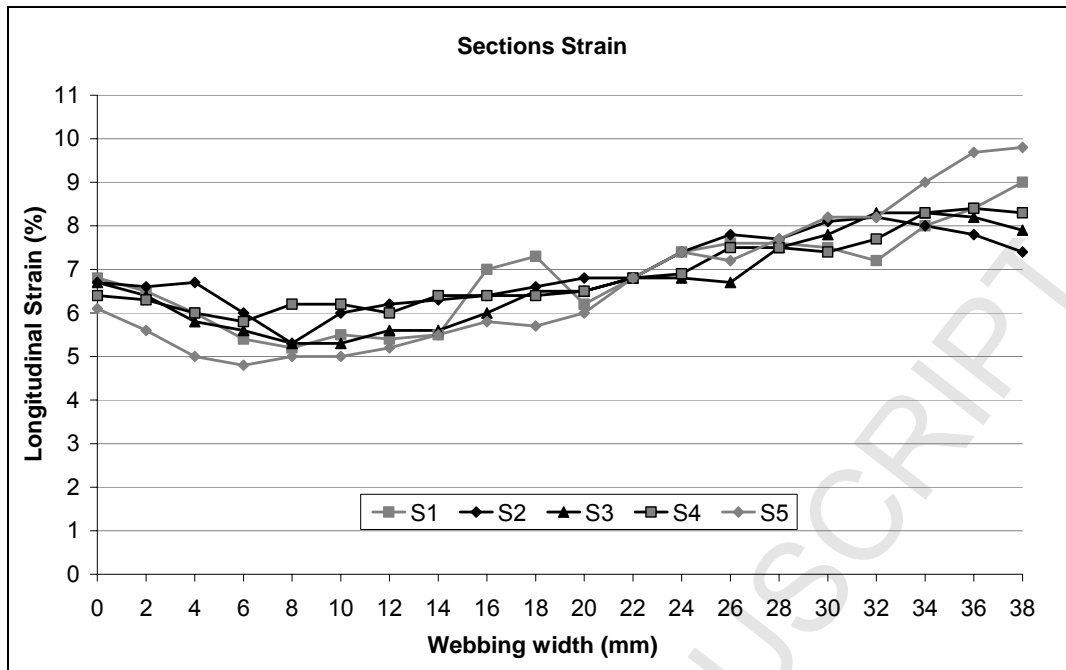


Fig. 15. Longitudinal strain distributions for different sections of the webbing at 67mm

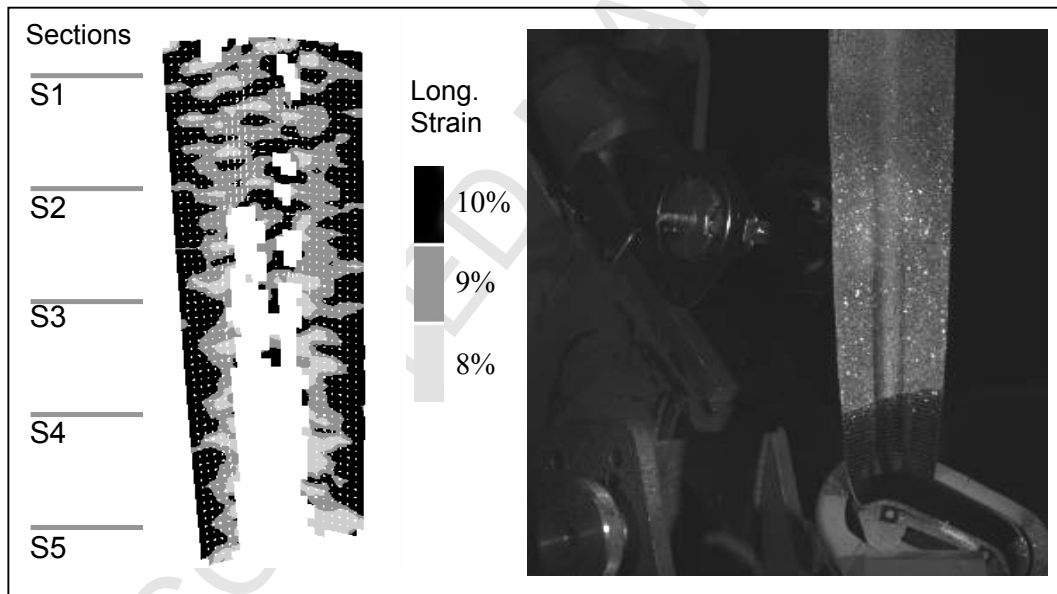


Fig. 16. Variation of the longitudinal strain distribution at 83mm

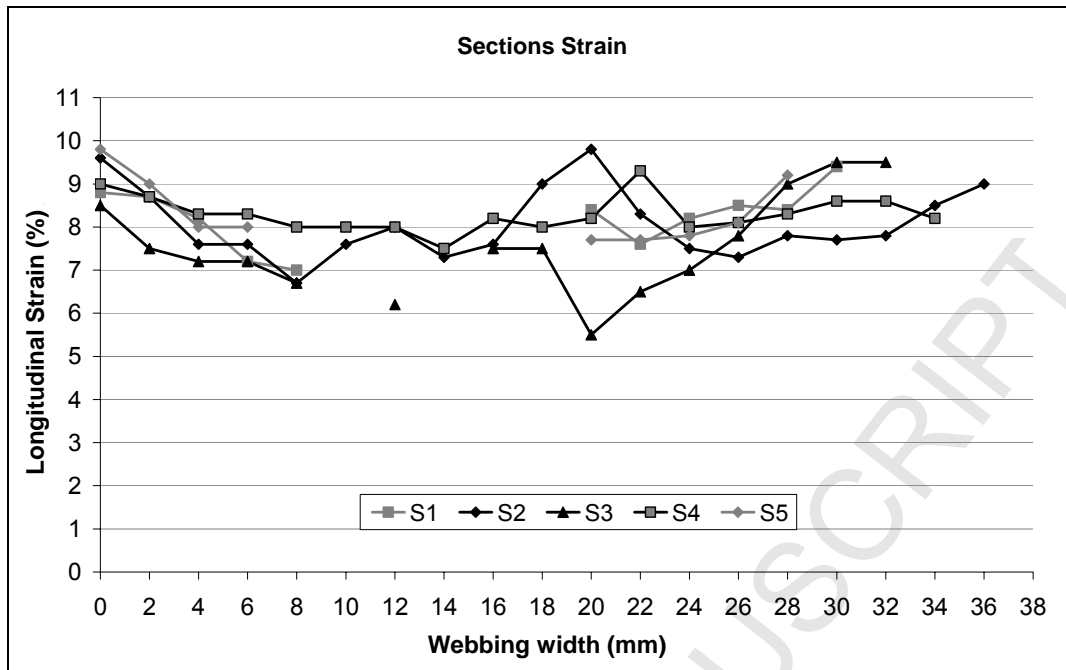


Fig. 17. Longitudinal strain distributions for different sections of the webbing at 83mm

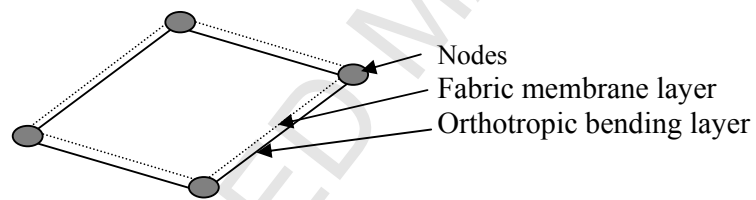


Fig. 18. Two layers Finite Element

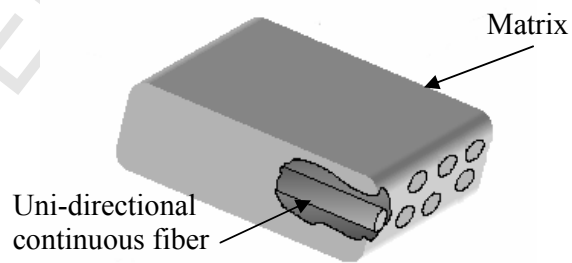


Fig. 19. Sketch of a composite ply

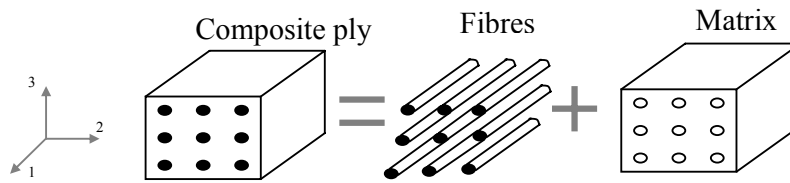


Fig. 20. Bi-phase rheological composite model

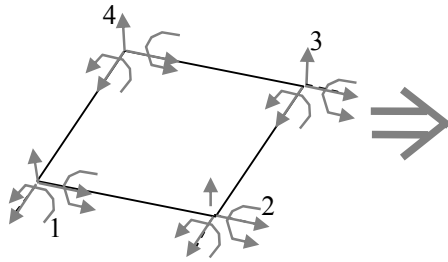


Fig. 21. Shell element decomposition to plate-bending element

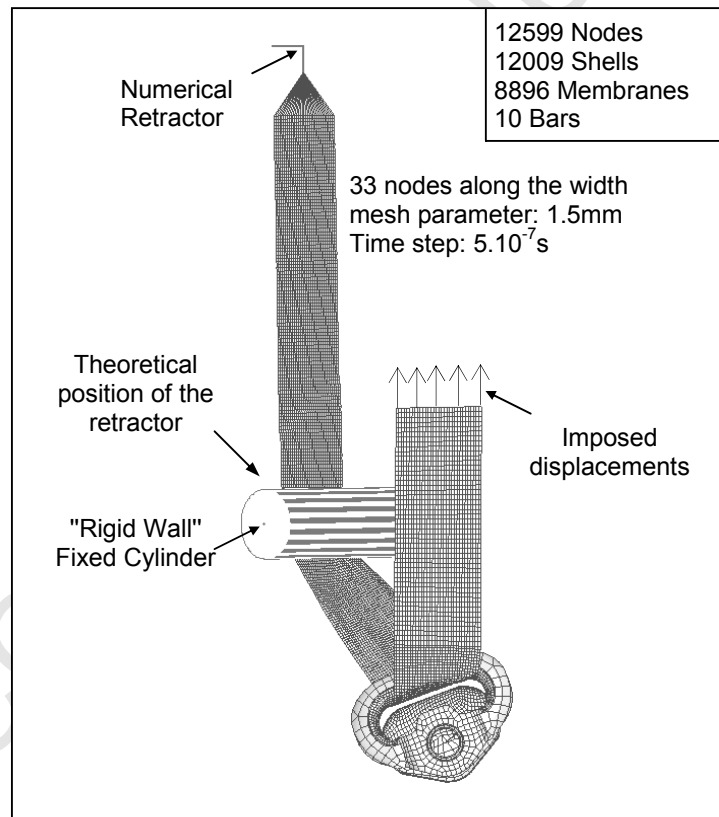


Fig. 22. WGRAT model (orientation 45°/45°)

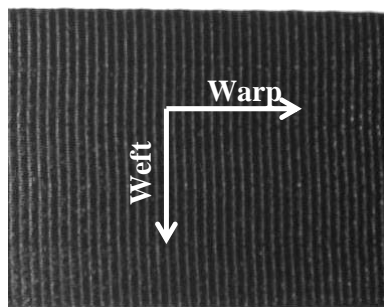


Fig. 23 Warp / weft directions

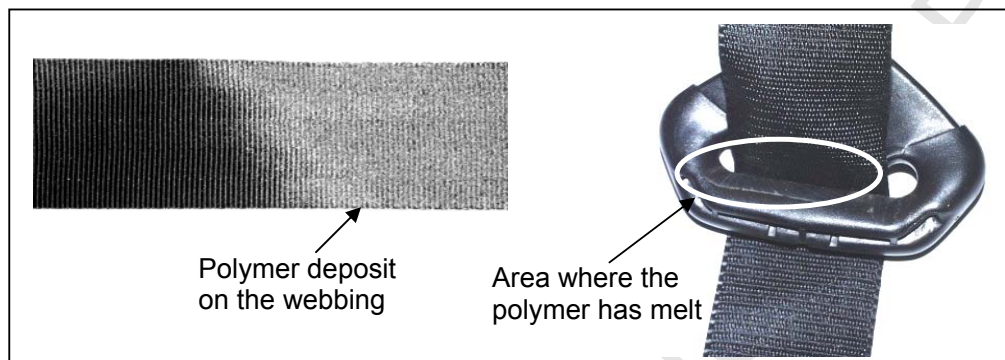


Fig. 24 Melted polymer deposit on webbing

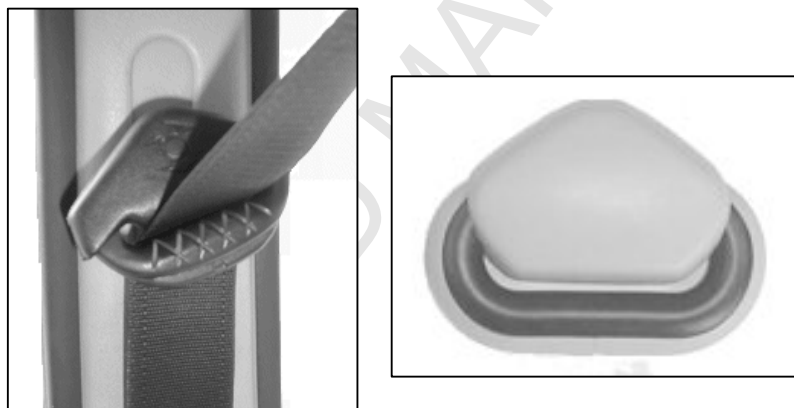


Fig. 25 Two types of sliding surfaces

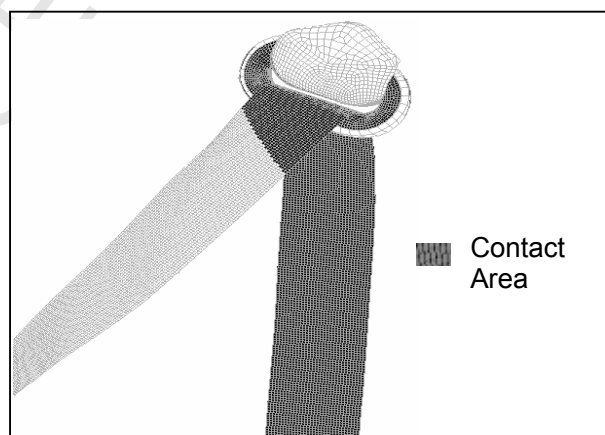


Fig. 26 Contact Area

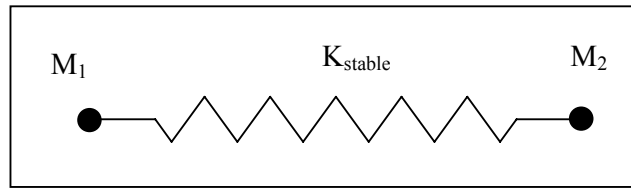


Fig. 27 1 D.O.F. system

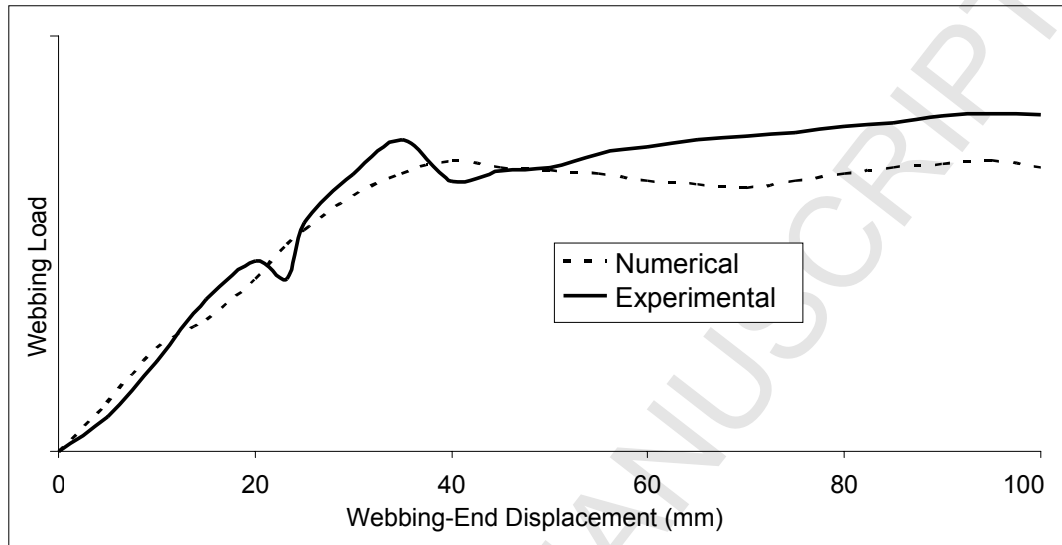


Fig. 28 Comparison of webbing load levels - Numerical / Experimental

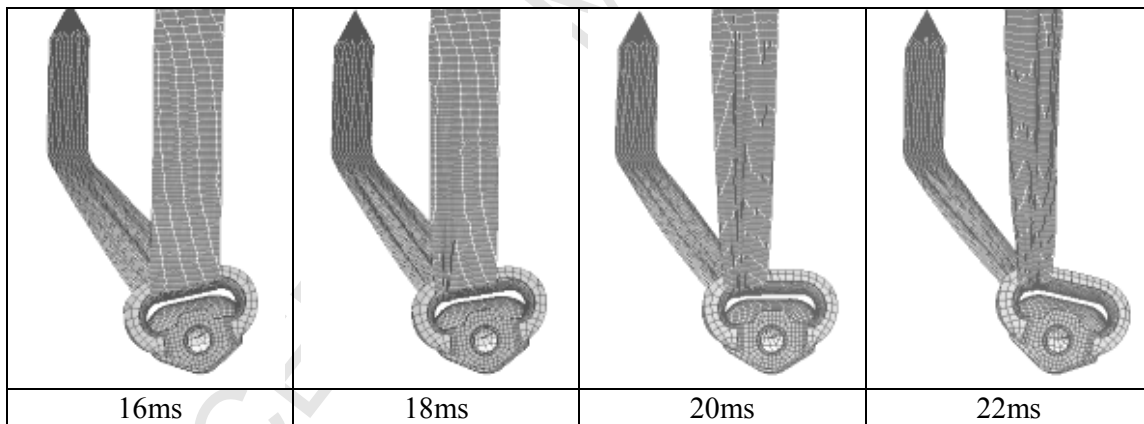


Fig. 29 Bunching case with the WGRAT

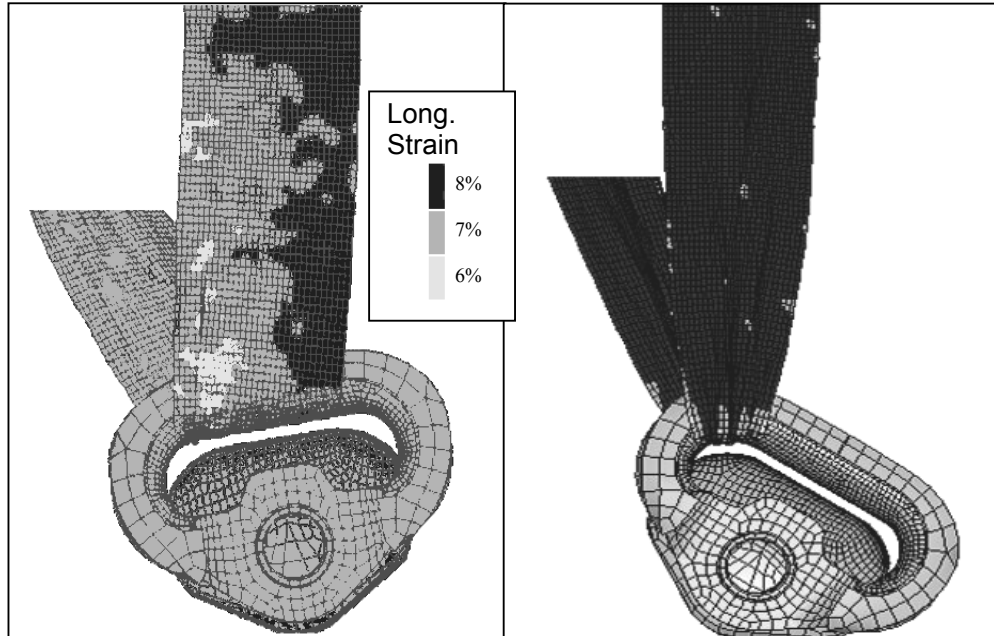


Fig. 30 Strain distributions through the vertical webbing portion at 17-22ms